Applied Magnetic Resonance (2024) 55:987–1010
https://doi.org/10.1007/s00723-024-01685-5

Applied
Magnetic Resonance

REVIEW

EPR in Research of the Magnetic Properties of Spin-Crossover Fe(III) Complexes with Polydentate Schiff Bases

E. N. Frolova[1] · O. A. Turanova[1] · L. V. Bazan[1] · I. V. Ovchinnikov[1] · A. N. Turanov[1]

Received: 29 March 2024 / Revised: 9 July 2024 / Accepted: 14 July 2024 /
Published online: 26 July 2024

Abstract

Schiff bases allow the creation of compounds with a wide variety of architectures and properties and have been of interest to researchers for many years. This mini-review describes some of the possibilities of the EPR method, which we use to study Fe(III) complexes with polydentate Schiff bases, many of which have been synthesized for the first time. Obtaining information at the local level using EPR spectroscopy allows us to grasp the molecular structure–property relationship and to adjust the synthesis strategy to create multifunctional substances with predetermined properties.

Abbreviations

Salen	Dianione *N*,*N*´-ethylenebis(salicylaldimine), N2O2 donor atoms
Acen	Dianione *N*,*N*´-ethylenebis(acetylacetonylideneimine), N2O2 donor atoms
Bzacen	Dianione N,N´-ethylenebis(benzoylacetonylideneimine), N2O2 donor atoms
Salten	Dianione *N*,*N*´-bis[(2-hydroxy-phenyl)methylene]-4-azaheptane-1,7-diaine, N3O2 donor atoms
$C_{18}H_{37}O$-salten	Dianione bis[(2-hydroxy-4-octadecyloxyphenyl)methylene]-4-azaheptane-1,7-diamine, N3O2 donor atoms
CH_3him	N-methylimidazole, N donor atom in mononuclear complexes, N2 in polynuclear complexes
Pic	4-Methylpyridine, N donor atom
Tvp	1,2-Di(4-pyridyl)ethylene, N2 donor atoms
Sp	4-Styrylpyridine, N donor atom
Qsal	Anione N-(8-quinolyl)-salicylaldimine, N2O donor atoms

✉ A. N. Turanov
sasha_turanov@rambler.ru

[1] Zavoisky Physical-Technical Institute, FRC Kazan Scientific Center of RAS, Kazan, Russia

3-CH_3O-qsal	Anione N-(8-quinolyl)-3-methoxysalicylaldimine, N2O donor atoms
Saleen	Anione salicylidene-N'-ethyl-N-ethylenediamine, N2O donor atoms
4-CH_3O-saleen	Anione 4-methoxysalicylidene-N'-ethyl-N-ethylenediamine, N2O donor atoms

1 Introduction

Coordination compounds of transition group metals with polydentate organic ligands are promising for the creation of new materials. The most used ligands are Schiff bases [1]. This is explained by the relative simplicity of synthesis, the wide possibility of varying the substituents, as well as the possibility of constructing mono- and polynuclear coordination compounds with different geometry of the coordination unit, possessing a wide range of physicochemical properties.

One of the most interesting phenomena of coordination chemistry is molecular bistability and spin crossover (SCO). It is observed in transition metal complexes with the d^4–d^7 electronic configuration in the presence of the corresponding ligand field. Under weak external influences (change of temperature, pressure, light irradiation, etc.), metal ions in the molecule change their spin state [2, 3], which is associated with a change in the structure of the coordination compound and leads to the appearance of new magnetic and optical properties of the whole substance.

For this reason, the study of SCO materials is promising for the development of technical devices such as displays and memory devices, molecular magnetic devices, sensors, and as components of multifunctional materials [4–6].

Iron(III) compounds have an advantage over the more studied iron(II) systems in that they are generally stable in air and can, therefore, be expected to be more sought after in practical devices.

Various physical methods are used to detect and investigate spin-variable properties: magnetometry, optical and vibrational spectroscopy, Mössbauer spectroscopy, crystal structure, and heat capacity determination.

The SCO phenomenon is accompanied by a change in the magnetic susceptibility of a substance both in the solid state and in solutions. Measurement of the magnetic susceptibility of a complex as a function of temperature $\chi(T)$ and determination of its magnetic moment is the most popular method for studying the spin state of a substance.

The vast majority of studies on the magnetic properties of Fe(III) complexes have been performed for solids [3, 7]. Much less attention is paid to solutions, although the magnetic properties of complexes in solutions can vary widely [8–10]. The magnetic susceptibility in solutions is measured by magnetometry methods, including nuclear magnetic resonance (NMR) spectroscopy using special ampoules with special shapes: Evans method, spherocylindrical ampoule method, rectangular ampoule method, etc. [11–14].

Magnetometry is an "integral" method, i.e., the measurement result is averaged over the whole sample, including contributions from different ions; it depends

both on the number and ratio of these ions and on the states in which the ions are located. In complex systems containing only iron ions, transitions between states with different valence and spin are possible, for example, transitions between divalent ions ($S=0 \Leftrightarrow S=2$) and trivalent ions ($S=1/2 \Leftrightarrow S=5/2$) [15]. Moreover, the "integrality" of the method also consists in the fact that the measurement summarizes the contributions from all electronic levels, the occupancy of which depends not only on temperature, but also on many other external factors. Thus, the interpretation and analysis of the obtained results become more complicated and may lead to ambiguity.

Spin variable compounds are often, but not always, characterized by the phenomenon of thermochromism: color change with temperature. This is easily controlled by UV–Vis spectroscopy. The example of Fe(III) complexes shows that the high-spin (HS) state is characterized by absorption in the region 510–550 nm, while the absorption of the low-spin (LS) state is shifted to the long wavelength region and can be in the range from 640 to more than 800 nm [13, 14, 16–21].

One of the methods for studying SCO systems is Mössbauer spectroscopy [22, 23]. ^{57}Fe nuclei of different valence and with different spins absorb gamma quanta of different energies, and the ability to resolve the fine structure of energy levels provides rich information not only about the iron atoms themselves, but also about their nearest chemical environment. However, due to the low specific content of iron atoms in organometallic complexes, the synthesis of samples enriched in ^{57}Fe isotopes is required for studies in a wide range of temperatures, which is a significant limitation in the application of this method.

Structural studies of a large number of spin-variable Fe(III) compounds by X-ray diffraction analysis have shown that the metal–ligand bond length is longer in the HS state than in the LS state [24–26]. The single-crystal X-ray diffraction study also provides answers about intermolecular interaction, possible hydrogen bonds and π–π interactions. The disadvantage of the method is that it is not always possible to grow a single-crystal suitable for studies.

Electron paramagnetic resonance (EPR) spectroscopy is a unique highly sensitive method for studying the local magnetic and structural properties of the Fe(III) ion and its environment [27]. It is free from the limitations listed above. Therefore, the combination of EPR spectroscopy with other methods of investigation allows a deeper understanding and evaluation of changes in intramolecular and intermolecular interactions occurring during the spin transition.

We have been applying EPR to the study of Fe(III) SCO compounds for a number of years. The diagram demonstrates the very high publication rate of studies using the EPR method (Diagram 1**a**) clearly, as well as systems with SCO properties (Diagram 1**b**), but there are very few publications that describe the application of EPR to study the properties of SCO systems (Diagram 1**c**).

There are disastrously few review papers on EPR compared to NMR [28, 29]. There are no reviews on the application of EPR spectroscopy in the study of the SCO of Fe(III) compounds in the literature; accordingly, one of the goals of this work is to stimulate research in this area by other scientific groups. In the

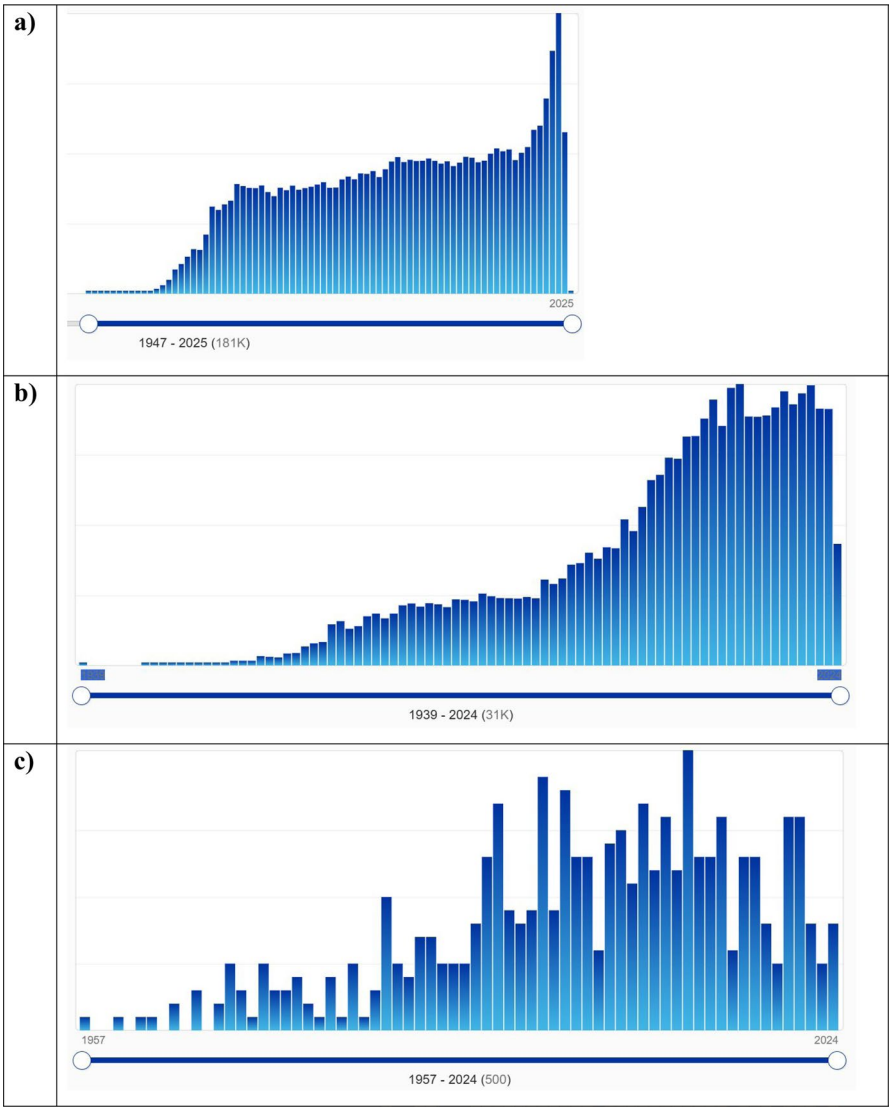

Diagram 1 Dependence of the number of scientific publications per year vs. the year of publication according to SciFinder: **a** query "EPR"; **b** query "SCO"; **c** query "EPR + SCO". The total number of publications is indicated in brackets

presented mini-review, we will touch upon some of the capabilities of the method, which we have used in analyzing the structure and magnetic properties of Fe(III) compounds with tri-, tetra- and pentadent Schiff bases. CW EPR spectra in the X- and Q-bands were analyzed to determine the parameters, and the capabilities of the EasySpin software package [30] were used to simulate the spectra.

1.1 Fe(III) Ions in a High-Spin (HS) State ($^6A_1$ $S=5/2$)

In the EPR spectra of the studied complexes, a number of lines corresponding to Fe(III) ions in the high-spin state (electronic configuration d^5, $S=5/2$) were found, which are described by the spin Hamiltonian:

$$\widehat{H} = g\beta HS + D\left[\widehat{S}_Z^2 - \left(\frac{1}{3}\right)S(S+1)\right] + E\left(\widehat{S}_X^2 - \widehat{S}_Y^2\right) \quad (1)$$

Here, D and E are the tetragonal and rhombic zero-field splitting parameters. If the electron Zeeman energy is larger than the zero-field terms ($h\nu >> D$, $E=0$), then $(2S+1)$ resonances from all levels of the fine structure are observed at the value of free spin g. If ($D >> h\nu$) the three Kramers' doublets are well separated and the EPR signal within each of them can be described by the effective spin $S_{\text{eff}}=1/2$ and the values of the effective g factor g_{eff} according the methodology of Refs. [31, 32]. If the system is tetragonal ($E=0$) and only transitions within the ground state are allowed, doublet resulting in resonances at $g_{\|}=2.0$ and $g_{\perp}=6.0$. In the case of the limiting rhombic symmetry ($E/D=1/3$), an isotropic line with $g_{\text{eff}}=4.3$ is recorded in the EPR spectrum, due to the medium of the three Kramers doublets, and a weak signal with $g_{\text{eff}} \approx 9.6$, due to the lower doublet. In other cases, the EPR spectrum has a more complex shape, since the arrangement of fine structure lines depends on both the magnitude and the relationship between the values of $h\nu$ and the parameters D and E.

An example of commonly observed spectra is shown in Fig. 1a [33], the effective parameters of the main signal **A** $g_{\text{eff}} \approx 4.2$ correspond to the Fe(III) centers with the fine structure parameter ($D > h\nu$) and orthorhombic distortions $E/D \approx 1/3$ [33]. The lines of transition between the sublevels of the lowest doublet are much less intense because of their large anisotropic width. They appear as a "shoulder" of the main signal at weak fields with $g_{\text{eff}} \approx 9$. The fine structure parameters determined for some complexes in the HS state are given in Table 1 (Schemes 1, 2, 3).

It was found that the shape of the EPR spectrum of the compound [Fe(salen)$(sp)_2$]BPh_4·MeOH (Scheme 4a) demonstrates an appreciable temperature dependence, which indicates a change in the symmetry of the crystal field on the central ion ([14], see Fig. 1b). According to the spectra simulation results, there are two main HS conformations, which are characterized by different values of the rhombic distortion of the complex symmetry: $E/D \sim 0.065$–0.095 (I) and $E/D \sim 0.19$–0.22 (II). At low temperatures, the conformation **II** dominates (about 80% of the complexes at 4 K). With increasing temperature, the percentage of conformation **I** increases so that at temperatures above 160 K, it becomes predominant. At high temperature, the lines broaden and a signal with intermediate g_{eff} values appears, which can be explained by an increase in the transition rate between the two conformations. In the Q-band EPR spectrum, the resolution of signals by g factor was found, which allows us to estimate the value of $D \approx 0.33$ cm^{-1}.

The integral intensity of the lines of the EPR spectrum is proportional to the static magnetic susceptibility χ, so its temperature behavior is one of the sources of information about the spin and magnetic state of the system. When studying

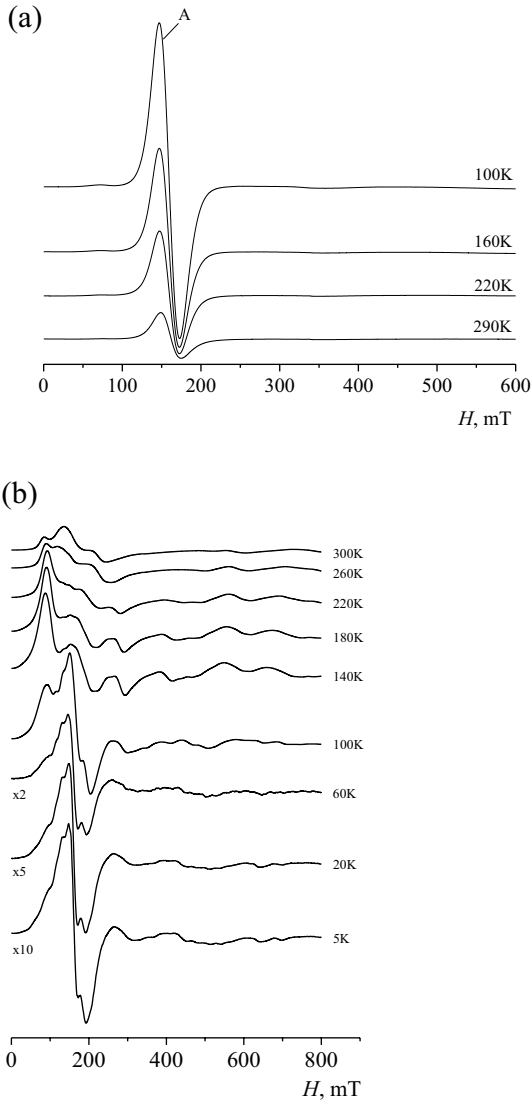

Fig. 1 Temperature plots of the EPR spectra of complex [Fe(salten)him]BPh_4 (**a**) [33] and [Fe(salen)$(sp)_2$]BPh_4·MeOH (**b**) [14]

Table 1 The fine structure parameters for some complexes in the HS state

Complex	D, cm^{-1}	E/D	Ref	Scheme
[Fe(salen)$(CH_3him)_2$]BPh_4	0.35	~0.16	[34]	1
[Fe(salen)$(CH_3him)_2$]BF_4	0.35	~0.16	[34]	
[Fe(salen)$(CH_3him)_2$]ClO_4	0.35	~0.16	[34]	
[Fe(salen)(tvp)] BPh_4·$2CH_3OH$	0.32	0.27	[21]	2
[Fe(4-CH_3O-saleen)$_2$]PF_6	> 0.3	0.22	[35]	3

Scheme 1 Schematic representation of the molecule structure of $[Fe(salen)(CH_3him)_2]^+$

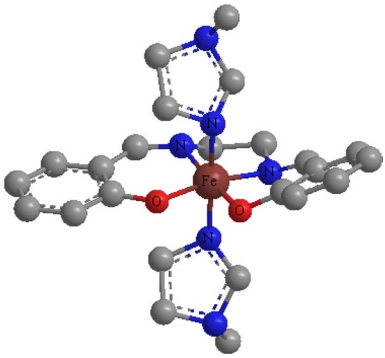

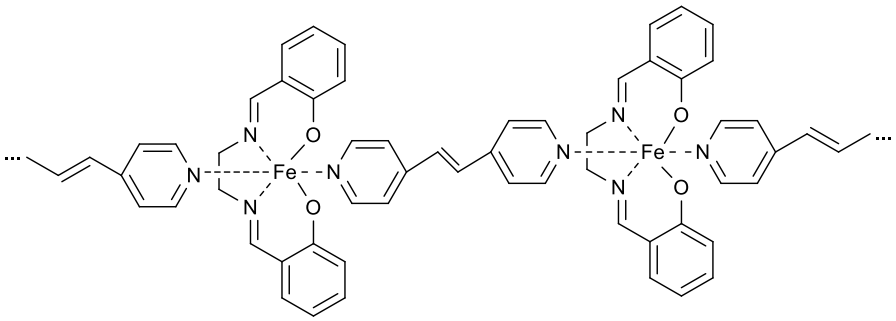

Scheme 2 Schematic representation of the molecule structure of $[Fe(salen)(tvp)]^+$

Scheme 3 Schematic representation of the molecule structure of $[Fe(4\text{-}CH_3O\text{-}saleen)_2]PF_6$

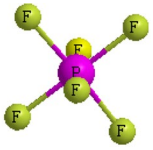

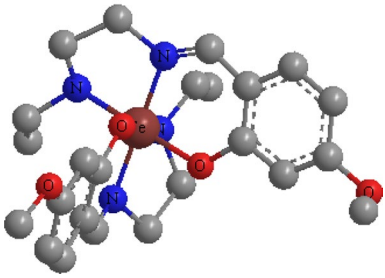

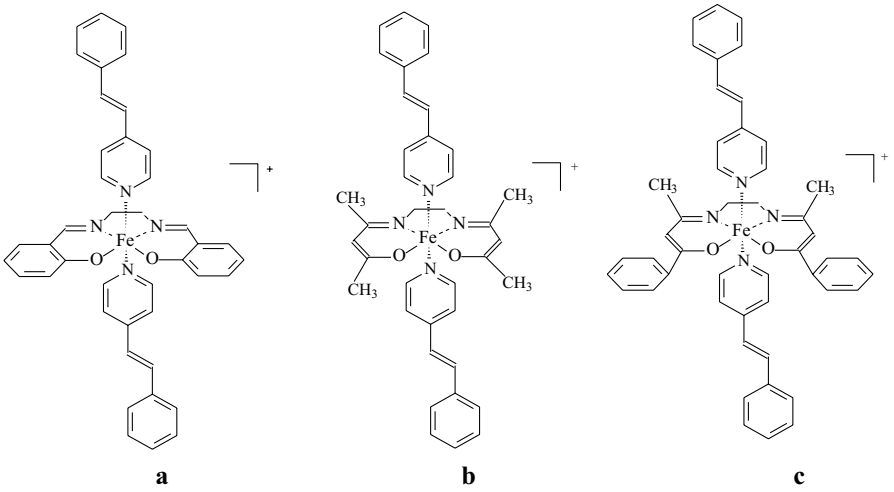

Scheme 4 Schematic representation of the molecule structure of $[FeL(sp)_2]^+$. **a**) L = salen, **b**) L = acen, **c**) L = bzacen

exchange interactions between Fe(III) ions in complex compounds, the combination of EPR spectroscopy and magnetic susceptibility measurements is quite fruitful.

It has been shown by EPR and magnetometry that the complexes of the studied precursor [Fe(salten)Cl] (Scheme 5) in polycrystalline samples have a high-spin state $S = 5/2$. It was found that along with individual metal centers with large fine structure parameters D and different degrees of orthorhombic distortions, exchange-bonded clusters with an anomalous temperature dependence of the

Scheme 5 Schematic representation of the molecule structure of [Fe(salten)Cl] in a crystal according to crystallography data [36]

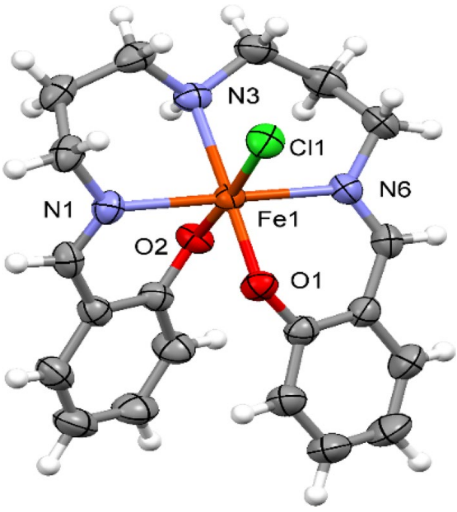

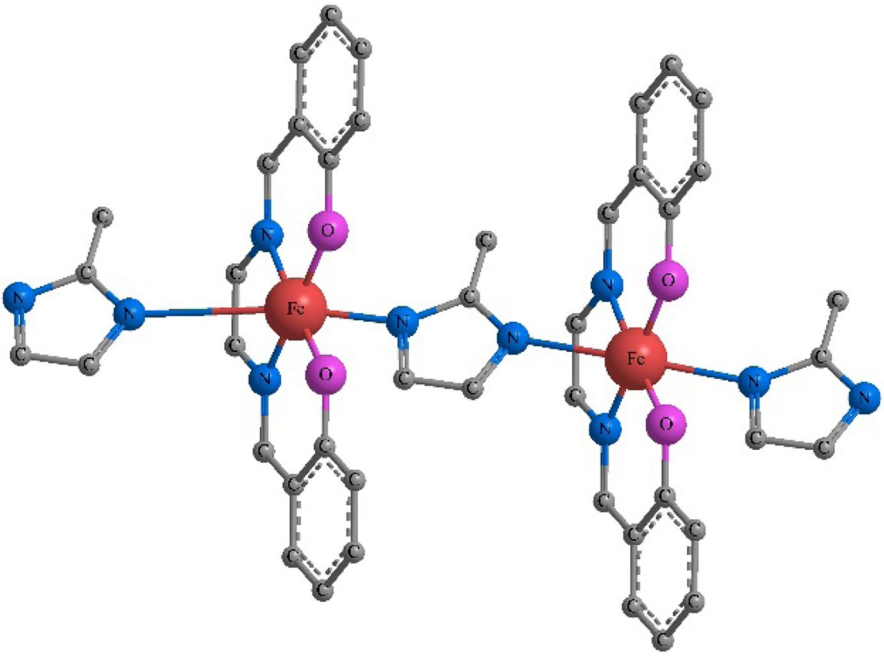

Scheme 6 Schematic representation of the molecule structure of $[Fe(salen)(2\text{-}CH_3\text{-}him)]_n$

integral line intensity appear in the samples obtained under different conditions, and there is no EPR signal from the bulk of the introduced Fe(III) ions [36].

Valuable data were obtained by analyzing the integrated intensity of EPR signals of HS complexes in [34]. A distinct behavior of the integrated intensity below 10 K was found for samples with different types of outer-sphere ions (BPh_4, BF_4, and ClO_4). Magnetization measurements confirmed the HS state of Fe(III) ions in the samples and established that the contribution of χ_0 to the Curie law, independent of temperature, is negative or positive depending on the nature of the outer-sphere ion.

A significant deviation of the temperature dependence of the integral intensity from the Curie–Weiss law was found for one of the signals in the EPR spectrum $[Fe(salen)(2\text{-}CH_3\text{-}him)]_n$ (Scheme 6, Fig. 2 [37]). It has a broad peak at $T_{max} = 100$ K and can be interpreted as a result of exchange in a chain of bound centers. The dependence was modeled in the framework of an infinite linear chain model with isotropic exchange interaction ($H = 2J \sum_{ij} S_i S_j$) between Fe(III) ions based on the expressions proposed in Refs. [38, 39]:

$$\chi = \frac{NS(S+1) \cdot g^2 \cdot \mu_B^2}{3k_B T} \frac{1+u(x)}{1-u(x)} \tag{2}$$

$$u(x) = \coth(x) - 1/x \tag{3}$$

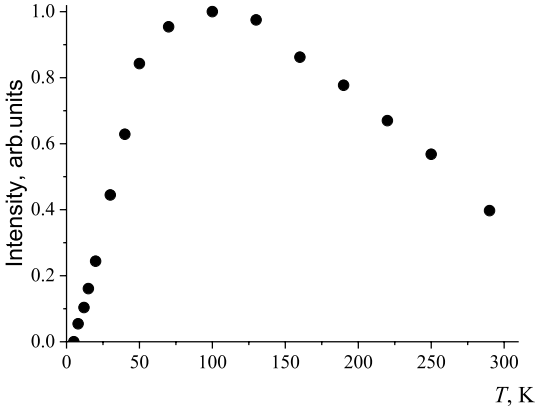

Fig. 2 Temperature dependences of integral intensity of a signal with $g_{eff} \approx 2.0$ of the EPR spectra of complex [Fe(salen)(2-CH_3-him)]$_n$ [37]

$$x = -2JS(S+1)/k_BT. \tag{3}$$

Here, k_B is the Boltzmann constant, μ_B is the Bohr magneton, $g=2.000$, $S=5/2$, $J>0$ corresponds to antiferromagnetic exchange interactions.

The position of the temperature dependence peak corresponds to the exchange interaction $2J_1=17$ cm^{-1} [37]. Comparison of the results obtained by EPR with the magnetic susceptibility data made it possible to separate the contributions from the antiferromagnetic interaction inside different chains ($2J_1=17$ cm^{-1} and $2J_2=1.6$ cm^{-1}) and the ferromagnetic contribution (χ_0=-0.053 cm^3/mol) resulting from the zigzag packaging of complexes within the chain.

1.2 Fe(III) Ions in a Low-Spin (LS) State ($^2T_2$ $S=1/2$)

Figure 3 [34] exhibits the EPR signal typical for low-spin Fe(III) complexes. It should be note that parameters of the spin Hamiltonian were constant over the 5–340 K. Increase in temperature cause the broadening of the individual lines, reflected in the worsening of the spectral lines resolution up to practically isotropic spectral shape at $T>300$ K (Fig. 3). Such spectral changes point the increasing of relaxation contribution in the line width with the temperature increase.

The g factors of the observed signals of the LS Fe(III) complexes one can analyze within the single-electron approximation for the lower orbital triplet according to the approach described in Refs. [40, 41].

The relationships obtained with the use of the wave functions of the lower triplet with allowance made for the spin–orbit interaction $\xi\ \hat{l}\ \hat{s}$, as well as for the tetragonal (Δ) and orthorhombic (V) components of the ligand field are

$$\begin{cases} g_z = -2\left[A^2 - B^2 + C^2 + k\left(A^2 - C^2\right)\right] \\ g_x = 2\left[AC - B^2 + kB\sqrt{2}(C-A)\right] \\ g_y = -2\left[AC + B^2 + kB\sqrt{2}(C+A)\right] \end{cases}. \tag{5}$$

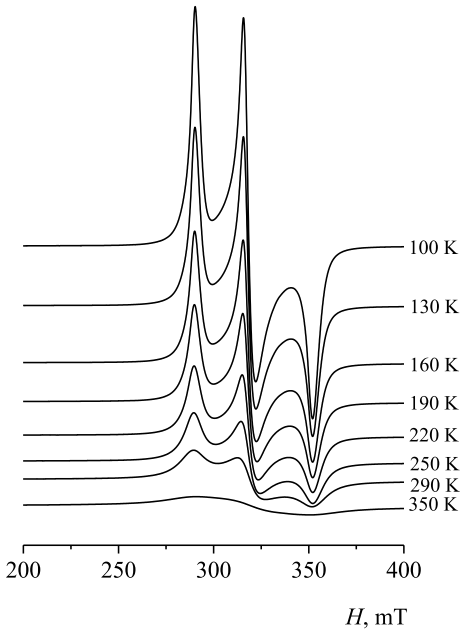

Fig. 3 Temperature dependences of the EPR spectra of complex $[Fe(acen)(him)_2]BPh_4$ [34]

Here, k is the orbital reduction parameter or covalency parameter and A, B, and C are the coefficients of the wave functions of the ground Kramers doublet:

$$\psi_1 = A\left|+1^+\right\rangle + B\left|\xi^-\right\rangle + C\left|-1^+\right\rangle, \tag{6}$$

$$\psi_2 = A\left|-1^-\right\rangle + B\left|\xi^+\right\rangle + C\left|+1^-\right\rangle, \tag{7}$$

$$|\xi\rangle \equiv \sqrt{\frac{1}{2}} \cdot \left[|+2\rangle - |-2\rangle\right], \tag{8}$$

where |+1>, |-1>, |ξ> are atomic orbitals, upper indices "+" and "−" are designations of spin states, and the normalization condition is

$$A^2 + B^2 + C^2 = 1. \tag{9}$$

The coefficients A, B, C, and k were calculated taking into account the tetragonal (Δ) and orthorhombic (V) components of the crystal field and the spin–orbit interaction. The values of E_i, Δ, and V were determined by substituting the obtained values into energy matrix and solving the corresponding system of linear equations (the value of ξ, was taken equal to − 460 cm^{-1}). Since the experimental results do not contain information on signs of the g_x, g_y, and g_z factors and their assignment to the x, y, and z molecular axes, the system of Eqs. (5) was solved for all possible 48 combinations, followed by the choice of a physically reasonable solution with

inclusion of recommendations [40–42]. The main criteria for the choice presents in Ref. [35]. The set of the g factors satisfying the system of Eqs. (5) with the least root-mean-square deviation from the experimentally determined g factors was determined by varying the parameters A, B, and C. For these theoretical g factors, which differ from the experimental g factors to a minimum extent, we derived the parameters of the ground-state wave function and the splittings in the crystal field. The wave functions of the ground doublet presented in the bases set of real wave functions, have the form:

$$\psi_1 = a\left|d_{yz}^{+}\right\rangle + b\left|d_{xy}^{-}\right\rangle + c\left|d_{xz}^{+}\right\rangle \tag{10}$$

$$\psi_2 = a\left|d_{yz}^{-}\right\rangle - b\left|d_{xy}^{+}\right\rangle - c\left|d_{xz}^{-}\right\rangle, \tag{11}$$

$$\left|d_{yz}\right\rangle \equiv \frac{i(|+1\rangle + |-1\rangle)}{\sqrt{2}}; \left|d_{xz}\right\rangle \equiv \frac{-(|+1\rangle - |-1\rangle)}{\sqrt{2}}; \left|d_{xy}\right\rangle \equiv \frac{-i(|+2\rangle - |-2\rangle)}{\sqrt{2}}. \tag{12}$$

The coefficients a, b, and c and the obtained parameters A, B, and C are related by the expressions:

$$a = -i(A + C)/\sqrt{2}, b = iB, c = (AC - A + C)/\sqrt{2}. \tag{13}$$

Thus, the EPR spectra parameters of the compounds in the LS states allowed us to estimate the wave functions of the ground state, the energy spacing between the orbital triplet levels, and the value of the tetragonal (axial) and the orthorhombic distortion of the complexes. The parameter values obtained on the basis of this analysis fit well with data from other methods (X-ray spectroscopy and DFT see, for example, Refs. [14, 21, 43]).

1.3 Bistable systems and spin transition

In octahedral complexes, Fe(III) ions can exist either in a high-spin state ($^6A_1$ $S = 5/2$) or in a low-spin state ($^2T_2$ $S = 1/2$) depending on the ratio between the splitting of the energy levels of the d electron in the cubic crystal field and the spin pairing energy. If the distance between the terms is of the order of the thermal energy (k_BT), then the SCO can be induced by the temperature.

In EPR spectra, the spin transition manifests itself in the characteristic dynamics of the signal shape (for example, Fig. 4a). In the general case, it consists of an increase in the relative intensity of the signal from high-spin complexes compared to the intensity of the signal from low-spin centers with increasing temperature. In some cases, in the presence of significant exchange interactions in the system and short spin–lattice relaxation times of $S = 1/2$ ions, the signal of the LS fraction may not appear and changes in the spectra are not so obvious (Fig. 4b, [44]). Valuable information about the parameters of the spin transition is provided by analysis of the

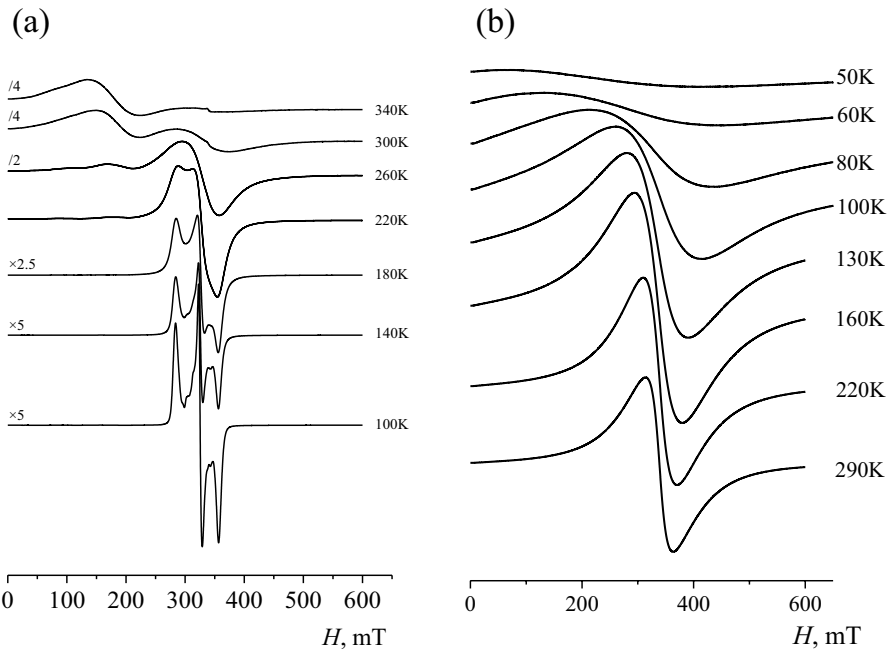

Fig. 4 Temperature dependences of the EPR spectra of complex $[Fe(acen)(sp)_2]BPh_4$ [14] (**a**) and $[Fe(acen)(pic)_2]BPh_4\ nH_2O$ [44] (**b**)

temperature variation of the integral intensities of both the overall EPR signal and the individual signals of the HS and LS fractions (Fig. 5).

The temperature at which the number of high-spin and low-spin centers in a system is equal is defined as the spin transition temperature ($T_{1/2}$). The temperature dependence of the high-spin fraction $\gamma_{HS}(T)$ is usually called the spin transition curve. Sometimes, to characterize the SCO, temperature dependences of the number of LS centers $\gamma_{LS}(T)$ or the γ_{HS} to γ_{LS} ratio are used. Spin transition curves have different shapes and are quite informative. Studies show that compounds with Schiff bases have SCO of different steepnesses and can demonstrate temperature hysteresis of magnetic and/or optical properties.

An interesting special case is the fact of the coexistence of HS and LS fractions in a wide temperature range without a registered SCO. Such bistable systems were discovered for $[Fe(3\text{-}CH_3O\text{-}qsal)_2]Y$ ($Y = PF_6$, BF_4, NCS, NO_3, BPh_4) (Scheme 7 a.) [45, 46]. The combined use of EPR and magnetic susceptibility methods allowed to establish the simultaneous existence of spatially separated high-spin and low-spin fractions in the studied compounds in the absence of spin transitions in each fraction. It was evidenced by the simultaneous presence of signals from HS and LS Fe(III) ions in EPR spectra and constant value of the product of magnetic susceptibility and temperature $\left(\chi_{mol} - \chi_0\right) \cdot T$ upon temperature variations, and the magnitude of this parameter, which is intermediate between those typical for HS and LS states of Fe(III) ions. LS fraction of all compounds reveals the antiferromagnetic correlations at low temperatures. HS fraction of complexes with $Y = PF_6$ demonstrate the weak

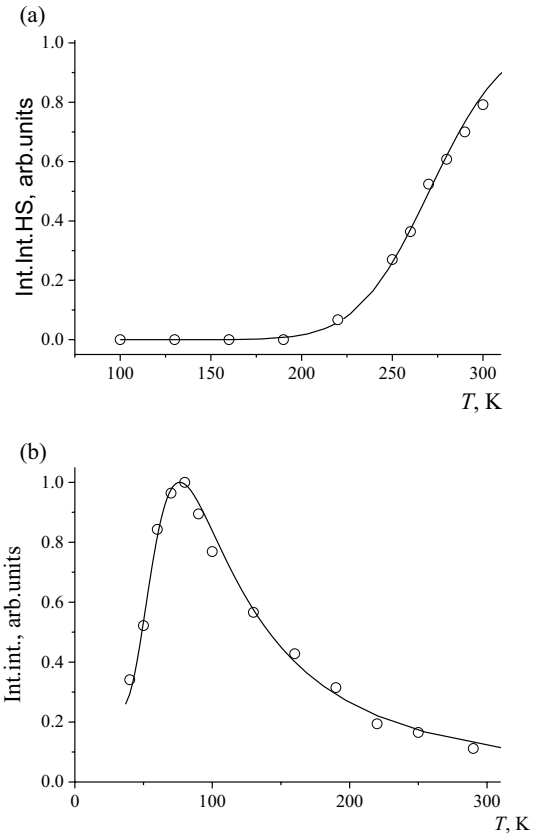

Fig. 5 Temperature dependences of the normalized integral intensity of the EPR signal (**a**) of HS fraction of [Fe(bzacen)(tvp)]$BPh_4 \cdot 2CH_3OH \cdot CHCl_3$ [47] and (**b**) of [Fe(acen)$(pic)_2$]BPh_4 nH2O [44]. Squares represent the experiment data, the line represents calculation results by Eq. (15), the thermodynamic parameters are presented in Table 2

ferromagnetic properties due to exchange interaction between complexes in whole temperature range. A considerable effect of outer-sphere anion on the spin state, the electronic properties of low-spin Fe(III) complexes was demonstrated.

The critical influence of a substituent in a Schiff base molecule qsal on the spin-variable properties of Fe(III) complexes in [Fe$(qsal)_2$]Y, Y = Cl, NCS, CF_3SO_3 (Scheme 7 b), was shown on the basis of EPR data and quantum chemical calculations as well [43]. Compound with Y = Cl is HS in the solid polycrystalline phase and goes into the LS state in diluted vitrified solution. Compound with Y = SCN exhibits SCO properties with magnetic hysteresis. Complex with Y = CF_3SO_3 remains in the LS state in the temperature range of 5–300 K. On the basis of the density functional calculations, the geometrical parameters of compounds in high- and low-spin states were optimized and the difference in their internal energies was calculated. Analysis of g factors of the observed LS Fe(III) complexes [43] (Table 2) was carried out using the single-electron approximation in the framework of the lower orbital triplet by the method described above.

The values of the spin–orbit coupling suppression parameter (k) significantly differ from unity, indicating strong covalent bonds in the observed LS complexes.

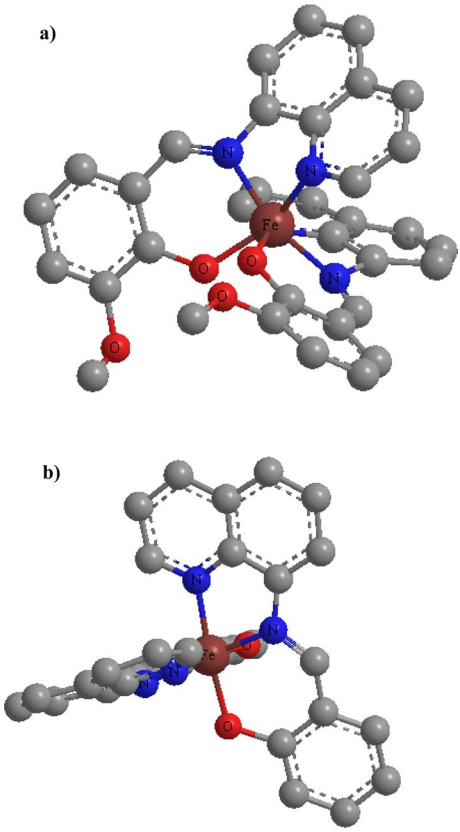

Scheme 7 Schematic representation of the molecule structure of **a**) $[Fe(3\text{-}CH_3O\text{-}qsal)_2]^+$, **b**) $[Fe(qsal)_2]^+$

Table 2 Results of the *g* factors of LS complexes analysis

Compound	g_x	g_y	g_z	K	Δ/ξ	V/ξ	$\Delta E_{12}/\xi$	$\Delta E_{13}/\xi$
$[Fe(qsal)_2]SCN$	2.205	2.187	1.917	0.647	2.007	0.068	5.657	6.654
$[Fe(qsal)_2]CF_3SO_3$	2.182	2.175	1.929	0.630	2.154	0.032	6.119	7.056
$[Fe(qsal)_2]Cl$ in toluene	2.192	2.184	1.935	0.686	2.271	0.038	6.457	7.405

Comparison of the axial (Δ) and rhombic (V) distortion parameters of the complexes, as well as the energy interval between the orbital triplet levels (ΔE_{12} and ΔE_{13}), show that the LS complexes with SCN have smaller degree of tetragonal distortion but stronger rhombic distortion compared to CF_3SO_3. The LS complex $[Fe(qsal)_2]Cl$ in vitrified toluene solution is characterized by smaller covalent bonding and larger axial splitting compared to the LS complexes in solid state.

It was found that the high-spin [Fe(salten)]Cl (Scheme 5) clusters in solution in acetonitrile break up into centers of high-spin and low-spin ($S = 1/2$) fractions, which coexist in the studied temperature range of 5–200 K [36]. The LS signals have different anisotropy of the *g* factor, and different values of the calculated

Scheme 8 Schematic representation of the molecule structure of [Fe(salten)(pic)]BPh_4

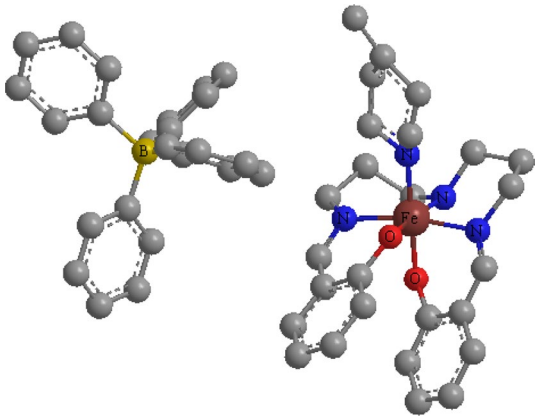

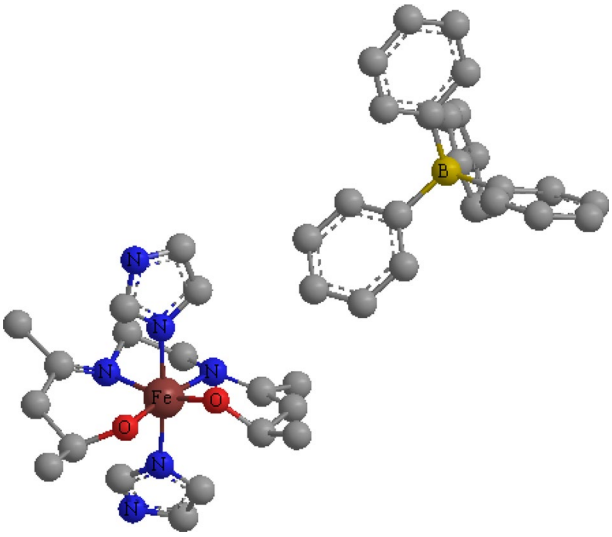

Scheme 9 Schematic representation of the molecule structure of [Fe(acen)$(him)_2$]BPh_4

orbital reduction parameter *k*. Note that the EPR spectra of vitrified diluted solutions (5–0.6 mmol/L) exhibit dipole–dipole interactions between metal centers, indicating the formation of weak molecular associates. The HS fraction in solution consists of six-coordinated pseudo-octahedral ($g_{eff} \approx 4$) and five-coordinated trigonal bipyramidal ($g_{eff} \approx 6$) Fe(III) complexes. A way for the appearance of LS centers observed in EPR spectra based on the concepts of supramolecular chemistry was proposed [36].

The magnetic properties of solutions of complexes [Fe(salten)Cl] (Scheme 5), [Fe(salten)(pic)]BPh_4 (Scheme 8) and [Fe(acen)$(him)_2$]BPh_4 (Scheme 9) in CH_2Cl_2 were analyzed [13]. The temperature dependences of μ_{eff} for the studied solutions of the complexes by NMR spectroscopy were obtained. Note, that the solutions of the

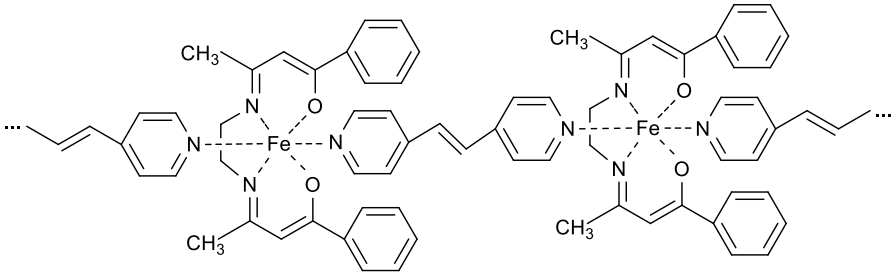

Scheme 10 Schematic representation of the molecule structure of $[Fe(bzacen)(tvp)]^+$

$[Fe(salten)(pic)]BPh_4$ and $[Fe(acen)(him)_2]BPh_4$ complexes demonstrated an incomplete SCO, the latter was mainly low-spin. It was revealed that in solutions studied SCO has a greater slope than that in the solid state.

In Ref. [14], the Fe(III) complexes with various tetradentate Schiff bases as the equatorial ligand and with 4-styrylpyridine as the axial ligands were characterized by the EPR and NMR methods. It was found that variation of the Schiff bases in the complex yield different spin states: high-spin for $[Fe(salen)(sp)_2]BPh_4$ (Scheme 4a) and SCO for $[Fe(acen)(sp)_2]BPh_4$ (Scheme 4b) and $[Fe(bzacen)(sp)_2]BPh_4$ (Scheme 4c).

It was revealed that in solutions, as well as in powders increase in the slope of SCO is observed in a series of the ligands salen → bzacen → acen. The fact that this trend persists both in polycrystalline powder samples and in solutions confirms the assumption that the SCO depends on the equatorial environment of the Fe(III) ion. A significant change in the shape of the EPR spectra for the powders in comparison with the vitrified solutions reflects the influence of the external environment of the complex (ice of the solvent or crystal lattice) on the symmetry of the coordination node, and as a result, on the SCO properties [14].

Analysis of the experimental data of LS centers of the $[Fe(bzacen)(tvp)]BPh_4$ complexes (Scheme 10) [47] allowed to establish differences in the immediate environment of the Fe(III) ion for samples with different numbers of solvate molecules and obtain energy level diagrams of complexes that explain the properties of SCO. In a number of cases, the thermodynamic parameters of the spin transition we determined from EPR data [21, 33, 35, 44, 47].

The changes in enthalpy and entropy that cause SCO can be determined by analyzing the temperature dependence of the integrated intensity. In the absence of a spin transition, the integral intensity of the HS isolated paramagnetic centers (I_{HS}) obeys Langevin equation and, in the high-temperature approximation, is inversely proportional to temperature. Note that the population of the HS state decreases with increasing temperature also according to Boltzmann's law of population of energy levels. At the same time, in SCO temperatures range, the relative content of HS centers (N_{HS}) increases with temperature. Taking into account the above processes, the experimentally observed change in the integral intensity of HS Fe(III) ions signal can be described by the equation:

$$I_{HS} = I_0 N_{HS}(T) \frac{\delta}{kT} \frac{\exp\left(-\Delta E / k_B T\right)}{1 + 2 \cdot \exp\left(-\Delta E / k_B T\right)}, \tag{14}$$

where ΔE is the energy interval between the ground (LS) end excited (HS) states of system, I_0 is the normalization factor, $\delta = \hbar \cdot \nu$ is the interval between levels, which are involved in the EPR signal formation.

The change in the relative content of the HS fraction $N_{HS}(T)$ during SCO corresponds to the thermodynamic relation [33]:

$$\ln\left(\frac{1 - N_{HS}}{N_{HS} - r}\right) = \frac{\Delta H + \Gamma \cdot \left(1 + r - 2N_{HS}\right)}{RT} - \frac{\Delta S}{R}, \tag{15}$$

where ΔH and ΔS are the changes of the enthalpy and entropy between HS and LS states, respectively; Γ is the parameter of interaction between HS and LS fractions; r is the residual HS fraction which is present at low temperatures in the LS fraction, $R \approx 8.31$ J·K^{-1}·mol^{-1} is the gas constant. The obtained values of the thermodynamic parameters of the spin transition of a number of compounds are given in Table 3 (Scheme 11).

The temperature hysteresis (with a width of 11 K) of the magnetic properties of Fe(III) complexes in the [Fe(4-OCH$_3$-saleen)$_2$]NO$_3$ (Scheme 12) compound was revealed in Ref. [35] (Fig. 6). The influence of the outer-sphere anions Y on these properties was discussed. The thermodynamic properties of the SCO were determined from the EPR data as well. The EPR spectra of the compounds with PF_6 and NO_3 counterions exhibit specific features that count in favor of the domain model of SCO. This correlates with rather large parameters Γ obtained from the experimental dependences of the relative content of HS complexes vis temperature. The higher parameter Γ for compound [Fe(4-OCH$_3$-saleen)$_2$]NO$_3$ suggests stronger intermolecular interactions and explains the existence of the abrupt spin transition accompanied by the hysteresis (see Table 3). It should be noted that the well-known condition for the appearance of the hysteresis $\Gamma > 2RT_{1/2}$ is satisfied fairly well for the studied compounds. The ability of the NO_3 anion to form hydrogen bonds with protons of methyl groups of neighboring complexes can enhanced the intermolecular interactions in the compound. This was confirmed

Table 3 The thermodynamic parameters of SCO of a number of compounds

Compound	$T_{1/2}$, K	$\Delta H/R$, K	$\Delta S/R$	Γ/R, K	r	Ref	Scheme
[Fe(salten)pic]BPh$_4$	~200	750	3.50	0	0.025	[33]	8
[Fe(acen)pic$_2$]BPh$_4$·nH$_2$O	~70	320	4.20	0	0	[44]	11
[Fe(bzacen)tvp]BPh$_4$·2CH$_3$OH·CHCl$_3$	285.8	3220	11.30	0	0	[47]	10
[Fe(bzacen)tvp]BPh$_4$·CH$_3$OH	208.4	1970	9.50	0	0.020	[47]	
[Fe(bzacen)tvp]BPh$_4$·nCH$_3$OH	328	2650	8.06	0	0.009	[21]	
[Fe(4-OCH$_3$-saleen)$_2$PF$_6$	211	3000	14.20	200	0	[35]	3
[Fe(4-OCH$_3$-saleen)$_2$NO$_3$	104↓ 115↑	2250	20.46	300	0	[35]	12

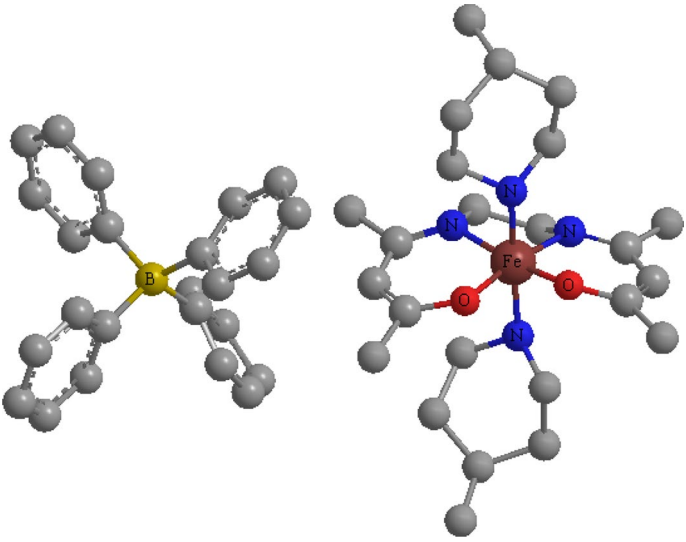

Scheme 11 Schematic representation of the molecule structure of $[Fe(acen)pic_2]BPh_4$

Scheme 12 Schematic representation of the molecule structure of $[Fe(4\text{-}OCH_3\text{-}saleen)_2NO_3$

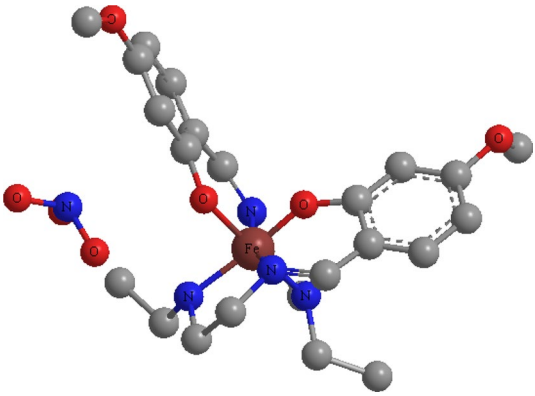

Fig. 6 Temperature dependences of the intensity of the EPR signal of $[Fe(4\text{-}CH_3O\text{-}saleen)_2]NO_3$. The solid line indicates the relative EPR intensity calculated according to the Curie law [35]

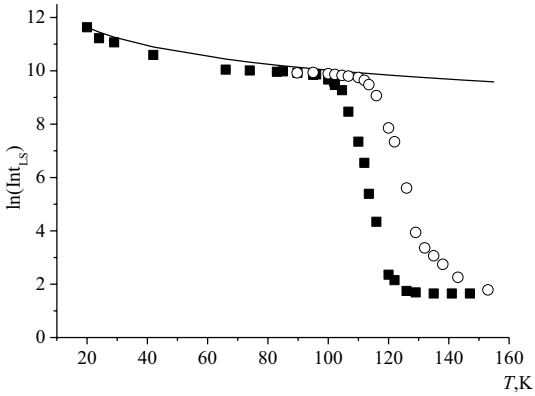

Scheme 13 Schematic representation of the molecule structure of $[Fe(saleen)_2]NO_3$

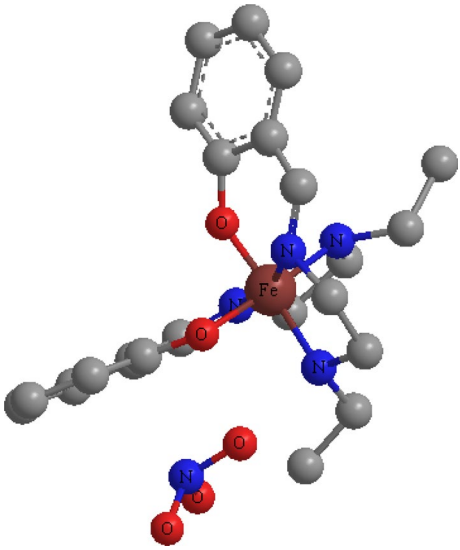

by the absence of the abrupt spin transition and hysteresis in the $[Fe(saleen)_2]NO_3$ (Scheme 13) compound that does not contain the CH_3O methoxy group [42].

An unusual field-induced spin instability leading to hysteresis of HS-LS composition in mesogenic systems of Fe(III) complexes $[Fe(4\text{-}C_{12}H_{25}O\text{-}saleen)_2]PF_6$ [48] has been found. The hysteresis may be due to the alignment of the systems by the magnetic field in the mesophase and full or partial orientational ordering upon cooling of the mesophase to the glassy state. In the spectra of HS complexes, the symmetrization of the crystal field around the Fe(III) ion was observed when the polycrystalline sample was first heated from room temperature to 400 K. The observed narrowing of the line (from 45 to 15 mT) at the crystal-smectic phase transition is explained by the increase in the intermolecular exchange interaction as a result of the structural rearrangement of the layers in the smectic phase.

The influence of the EPR-silent LS complexes is manifested in the broadening of the lines of the HS compounds when the temperature is decreased from 220 K. The introduction of the counterion SCN leads to a completely opposite situation: SCO is observed in the EPR spectra, but only signals from LS Fe(III) complexes are present [49]. Based on experimental data and quantum-chemical calculations, it was found that the totality of the observed features of the system is associated with the inclusion of the SCN group in the first coordination sphere of the Fe(III) ion.

EPR studies have revealed the possibility of SCO properties of liquid crystalline mono- and binuclear Fe(III) complexes with pentadentate Schiff base (salten) [50].

The magnetic properties of new seven-nuclear mixed-valence iron complexes $[Fe(II)(CN)_6\{Fe(III)(L)\}_6]Y_2$ with pentadentate ligands (L = salten, $C_{18}H_{37}O$-salten) and counter-anions (Y = Cl, NCS) (Scheme 14) have been studied by EPR and magnetometry methods [15]. The compound with NCS-counterion was found to possess the properties of SCO. The introduction of long octadecyloxy chains into the

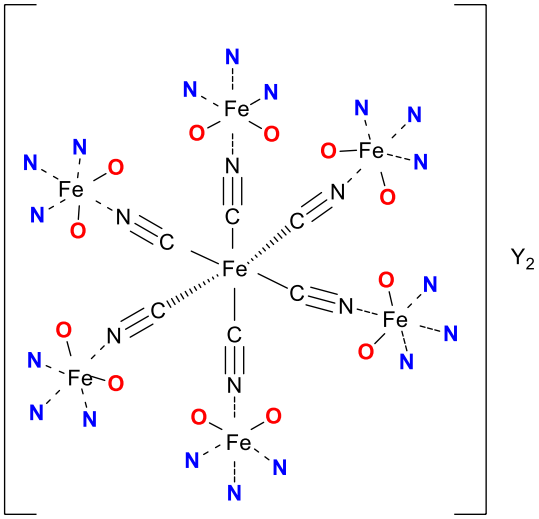

Scheme 14 Schematic representation of the molecule structure of $[Fe(II)(CN)_6\{Fe(III)(L)\}_6]Y_2$, L = salten or $C_{18}H_{37}O$-salten, Y = Cl, NCS

salten ligand leads to the appearance of thermotropic liquid crystalline properties and enhanced cooperative magnetic properties.

2 Conclusion

The spin state of an Fe(III) complex depends on its structure, which is determined by the composition and structure of the ligands, the type of counterion, the presence or absence of solvate within the complex, and the nature of intramolecular and intermolecular interactions. Each of these reasons causes redistribution of electron density on the ligands and affects the strength and symmetry of the ligand field, which can lead to changes in the spin-crossover properties of Fe(III) ions. To investigate the influence of the structure of coordination compounds on their magnetic properties, Fe(III) complexes with tri-, tetra- and pentadentate Schiff bases were obtained and studied. The combination of studies carried out by EPR, UV–Vis spectroscopy, magnetometry, and X-ray analysis provided information on the local symmetry and electronic structure of the spin-crossover synthesized Fe(III) complexes.

The mini-review describes some possibilities of the EPR method, which make it very effective in the study of local magnetic and structural properties of Fe(III) complexes with polydentate Schiff bases. Its contribution to the understanding and evaluation of changes in intramolecular and intermolecular interactions, including those occurring at spin transitions, is noted. We aimed that the data presented will be useful to researchers and will contribute to the successful application of EPR CW in the study of Fe(III) coordination compounds.

Acknowledgements EPR measurements were performed with the financial support from the government assignment for FRC Kazan Scientific Center of RAS.

Author contributions All the authors wrote the main manuscript text and reviewed the manuscript.

Funding Not applicable.

Data availability No datasets were generated or analysed during the current study.

Declarations

Conflict of interest The authors declare no competing interests.

Ethical approval Not applicable.

References

1. A.D. Garnovskii, I.S. Vasil'chenko, Russ. Chem. Rev. 71, 943 (2002). https://doi.org/10.1070/RC2002v071n11ABEH000759
2. Spin crossover in transition metal compounds (Vol. 1–3). Eds. P. Gutlich, H. A. Goodwin (2004 Springer Science & Business Media)
3. D.J. Harding, P. Harding, W. Phonsri, Coord. Chem. Rev. **313**, 38 (2016). https://doi.org/10.1016/j.ccr.2016.01.006
4. A. Galet, A.B. Gaspar, M.C. Munoz, G.V. Bukin, G. Levchenko, J.A. Real, Adv. Mater. **17**, 2949 (2005). https://doi.org/10.1002/adma.200501122
5. P. Gamez, J.S. Costa, M. Quesada, G. Aromí, Dalton Trans. **38**, 7845 (2009). https://doi.org/10.1039/B908208E
6. P. Gütlich, A.B. Gaspar, Y. Garcia, Beilstein J. Org. Chem. **9**, 342 (2013). https://doi.org/10.3762/bjoc.9.39
7. W. Phonsri, P. Harding, K.S. Murray, B. Moubaraki, D.J. Harding, New J. Chem. **41**, 13747 (2017). https://doi.org/10.1039/C7NJ03676K
8. C. Gandolfi, G.G. Morgan, M. Albrecht, Dalton Trans. **41**, 3726 (2012). https://doi.org/10.1039/C2DT12037B
9. P.N. Martinho, Y. Ortin, B. Gildea, C. Gandolfi, G. McKerr, B. O'Hagan, M. Albrecht, G.G. Morgan, Dalton Trans. **41**, 7461 (2012). https://doi.org/10.1039/C2DT12036D
10. W. Phonsri, P. Harding, L. Liu, S.G. Telfer, K.S. Murray, B. Moubaraki, T.M. Ross, G.N.L. Jameson, D.J. Harding, Chem. Sci. **8**, 3949 (2017). https://doi.org/10.1039/C6SC05317C
11. C.J. O'Connor, in Molecule-Based Magnetic Materials, ed. by M.M. Turnbull, T. Sugimoto, L.K. Thompson, 644, 44 (1996 American Chemical Society) https://doi.org/10.1021/bk-1996-0644.ch004
12. MYu. Volkov, O.A. Turanova, A.N. Turanov, Appl. Magn. Reson. **49**, 327 (2018). https://doi.org/10.1007/s00723-017-0970-1
13. MYu. Volkov, E.N. Frolova, L.V. Mingalieva, L.G. Gafiyatullin, O.A. Turanova, E.O. Milordova, I.V. Ovchinnikov, A.N. Turanov, Polyhedron **154**, 407 (2018). https://doi.org/10.1016/j.poly.2018.07.058
14. O.A. Turanova, MYu. Volkov, E.N. Frolova, L.V. Bazan, G.G. Garifzianova, L.G. Gafiyatullin, I.V. Ovchinnikov, A.N. Turanov, J. Chem. Phys. **151**, 014306 (2020). https://doi.org/10.1063/1.5124369
15. E.E. Batueva, A.R. Sharipova, E.N. Frolova, L.I. Savostina, L.V. Bazan, M.A. Cherosov, R.G. Batulin, O.A. Turanova, A.N. Turanov, Bull. Rus. Acad. Sci. Physics. 88, (2024) *accepted for publication*
16. K. Dankhoff, S. Schneider, R. Nowak, B. Weber, Z. Anorg, Allg. Chem. **644**, 1839 (2018). https://doi.org/10.1002/zaac.201800359
17. B. Djukic, P.A. Dube, F. Razavi, T. Seda, H.A. Jenkins, J.F. Britten, M.T. Lemaire, Inorg. Chem. **48**, 699 (2009). https://doi.org/10.1021/ic801233x
18. A. Ohyoshi, J. Honbo, N. Matsumoto, S. Ohta, S. Sakamoto, Bull. Chem. Soc. Jpn **59**, 1611 (1986). https://doi.org/10.1246/bcsj.59.1611
19. Y. Maeda, Y. Takashima, N. Matsumoto, A. Ohyoshi, J. Chem. Soc., Dalton Trans. 1115, (1986). https://doi.org/10.1039/DT9860001115

20. N. Matsumoto, K. Kimoto, A. Ohyoshi, Y. Maeda, Bull. Chem. Soc. Jpn **57**, 3307 (1984). https://doi.org/10.1246/bcsj.57.3307
21. O.A. Turanova, E.N. Frolova, L.G. Gafiyatullin, L.V. Bazan, A.N. Turanov, I.V. Ovchinnikov, Magn. Reson. Chem. **60**, 239 (2021). https://doi.org/10.1002/mrc.5223
22. V.G. Vlasenko, A.A. Guda, A.G. Starikov, M.G. Chegerev, A.V. Piskunov, I.V. Ershova, A.L. Trigub, A.A. Tereshchenko, Y.V. Rusalev, S.P. Kubrin, A.V. Soldatov, Eur. J. Inorg. Chem. **2021**, 756 (2021). https://doi.org/10.1002/ejic.202001033
23. W. Wen, Y.-Sh. Meng, Ch.-Qi Jiao, Q. Liu, H.-L. Zhu, Ya-M. Li, H. Oshio, T. Liu, Ang. Chem. Int. Ed. 59, 16393 (2020). https://doi.org/10.1002/anie.202005998
24. J.-T. Chen, X.-H. Zhao, Y.-Zhu Zhang, Dalton Trans. 49, 5949 (2020). https://doi.org/10.1039/D0DT00016G
25. R. Diaz-Torres, W. Phonsri, K.S. Murray, L. Liu, M. Ahmed, S.M. Neville, Ph. Harding, D.J. Harding, Inorg. Chem. **59**, 13784 (2020). https://doi.org/10.1021/acs.inorgchem.0c02201
26. J.J. Whittaker, Ph. Harding, J.K. Clegg, D.J. Harding, Cryst. Growth Des. **20**, 7006 (2020). https://doi.org/10.1021/acs.cgd.0c01073
27. S.A. Al'tshuler, B.M. Kozirev, *Electron Paramagnetic Resonance in Compounds of Transition Elements* (Wiley, New York, 1974)
28. J. Krzystek, A. Ozarowski, J. Telser, Coord. Chem. Rev. **250**, 2308 (2006). https://doi.org/10.1016/j.ccr.2006.03.016
29. K. Mobius, A. Savitsky, A. Schnegg, M. Plato, M. Fuchs, Phys. Chem. Chem. Phys. **7**, 19 (2005). https://doi.org/10.1039/B412180E
30. S. Stoll, A. Schweiger, J. Magn. Reson. **178**, 42 (2006). https://doi.org/10.1016/j.jmr.2005.08.013
31. H.H. Wickman, M.R. Klein, D.A. Shirley, J. Chem. Phys. **42**, 2113 (1965). https://doi.org/10.1063/1.1696253
32. R. Aasa, J. Chem. Phys. **52**, 3919 (1970). https://doi.org/10.1063/1.1673591
33. I.V. Ovchinnikov, T.A. Ivanova, O.A. Turanova, G.I. Ivanova, L.V. Mingalieva, A.A. Sukhanov, Rus. J. Coord. Chem. **39**, 598 (2013). https://doi.org/10.1134/S107032841308006X
34. T.A. Ivanova, L.V. Mingalieva, I.V. Ovchinnikov, O.A. Turanova, G.I. Ivanova, I.F. Gilmutdinov, Rus. J. Gen. Chem. **86**, 1647 (2016). https://doi.org/10.1134/S1070363216070197
35. T.A. Ivanova, I.V. Ovchinnikov, A.N. Turanov, Phys. Solid State **49**, 2132 (2007). https://doi.org/10.1134/S1063783407110194
36. E.N. Frolova, T.A. Ivanova, O.A. Turanova, L.V. Mingalieva, V.A. Shustov, E.M. Zueva, M.M. Petrova, A.T. Gubaidullin, I.V. Ovchinnikov, Rus. J. Inorg. Chem. **63**, 1012 (2018). https://doi.org/10.1134/S0036023618080077
37. T.A. Ivanova, O.A. Turanova, I.F. Gil'mutdinov, L.V. Mingalieva, I.V. Ovchinnikov, Rus. J. Inorg. Chem. 64, 520 (2019). https://doi.org/10.1134/S0036023619040119
38. R. Dingle, M.E. Lines, S.L. Holt, Phys. Rev. **187**, 643 (1969). https://doi.org/10.1103/PhysRev.187.643
39. R.L. Carlin, R. Burriel, J.A. Rojo, F. Palacio, Inorg. Chem. **23**, 2213 (1984). https://doi.org/10.1021/ic00183a001
40. M.M. Bhadbhade, D. Srinivas, Polyhedron **17**, 2699 (1998). https://doi.org/10.1016/S0277-5387(98)00039-4
41. T.L. Bohan, J. Magn. Res. **26**, 109 (1977). https://doi.org/10.1016/0022-2364(77)90240-2
42. M.S. Haddad, M.W. Lynch, W.D. Federer, D.N. Hendrickson, Inorg. Chem. **20**, 123 (1981). https://doi.org/10.1021/ic50215a028
43. T.A. Ivanova, I.V. Ovchinnikov, R.R. Garipov, G.I. Ivanova, Appl. Magn. Res. **40**, 1 (2011). https://doi.org/10.1007/s00723-010-0168-2
44. T.A. Ivanova, I.V. Ovchinnikov, I.F. Gil'mutdinov, L.V. Mingalieva, O.A. Turanova, G.I. Ivanova, Phys. Solid State, 58, 280 (2016). https://doi.org/10.1134/S1063783416020116
45. T.A. Ivanova, O.A. Turanova, L.V. Mingalieva, I.F. Gilmutdinov, I.V. Ovchinnikov, Magn. Res. Solids, Electronic Journal. 18, 16103 (2016).
46. T.A. Ivanova, O.A. Turanova, I.V. Ovchinnikov, L.V. Mingalieva, I.F. Gil'mutdinov, V.A. Shustov, L.G. Gafiyatullin, Rus. J. Inorg. Chem. 62, 476 (2017). 1134/S0036023617040076
47. T.A. Ivanova, I.V. Ovchinnikov, O.A. Turanova, L.V. Bazan, V.A. Shustov, R.G. Batulin, M.A. Cherosov, Magn. Reson. Chem. **58**, 949 (2020). https://doi.org/10.1002/mrc.5064
48. I.V. Ovchinnikov, T.A. Ivanova, V.E. Petrashen, Yu.G. Galyametdinov, G.I. Ivanova, Appl. Magn. Res. **29**, 325 (2005). https://doi.org/10.1007/BF03167020

49. I.V. Ovchinnikov, T.A. Ivanova, A.N. Turanov, R.R. Garipov, Phys. Solid State **51**, 2058 (2009). https://doi.org/10.1134/S1063783409100114
50. O.A. Turanova, G.I. Ivanova, L.G. Gafiyatullin, T.A. Ivanova, L.V. Mingalieva, A.N. Turanov, I.V. Ovchinnikov, Rus. J. Gen. Chem. **84**, 2174 (2014). https://doi.org/10.1134/S1070363214110218